Mimicking the magnetic properties of rare earth elements using superatoms

Shi-Bo Cheng[a], Cuneyt Berkdemir[a,b], and A. W. Castleman Jr.[a,c,1]

Departments of [a]Chemistry and [c]Physics, Pennsylvania State University, University Park, PA 16802; and [b]Department of Physics, Yildiz Technical University, Istanbul 34210, Turkey

Rare earth elements (REs) consist of a very important group in the periodic table that is vital to many modern technologies. The mining process, however, is extremely damaging to the environment, making them low yield and very expensive. Therefore, mimicking the properties of REs in a superatom framework is especially valuable but at the same time, technically challenging and requiring advanced concepts about manipulating properties of atom/molecular complexes. Herein, by using photoelectron imaging spectroscopy, we provide original idea and direct experimental evidence that chosen boron-doped clusters could mimic the magnetic characteristics of REs. Specifically, the neutral LaB and NdB clusters are found to have similar unpaired electrons and magnetic moments as their isovalent REs (namely Nd and Eu, respectively), opening up the great possibility in accomplishing rare earth mimicry. Extension of the superatom concept into the rare earth group not only further shows the power and advance of this concept but also, will stimulate more efforts to explore new superatomic clusters to mimic the chemistry of these heavy atoms, which will be of great importance in designing novel building blocks in the application of cluster-assembled nanomaterials. Additionally, based on these experimental findings, a novel "magic boron" counting rule is proposed to estimate the numbers of unpaired electrons in diatomic LnB clusters.

superatom concept | photoelectron imaging spectroscopy | rare earth elements | spin states | magic boron counting rule

Searching for low-cost and earth-abundant substitutes to replace precious and scarce elements or materials has become one of the major subjects in cluster science, which has attracted increasing research interest recently (1–5). It has been realized that the number of naturally occurring stable elements remains at 90, even if new elements, which usually have very short half-lives, continue to be added to the periodic table. Among these stable elements, some are very expensive or scarce (e.g., Pt and Au, which are widely applied as precious metal catalysts). Similarly, rare earth elements (REs), which are well-known for their optical and magnetic characteristics, are also expensive. In the meantime, some elements, like silicon, are highly abundant. Therefore, exploring ways to replace these precious or scarce elements in the periodic table is of significance in both fundamental and applied aspects. To achieve this objective, the superatom concept, which is an exciting achievement in cluster science (chosen stable clusters can mimic the chemistry of an atom or a group of the periodic table of elements and yet, retain their integrity when serving as building blocks of new materials), may be helpful. The key findings of this concept came from the experimental investigation of aluminum cluster reactivity performed by Castleman and coworkers in 1989, in which unusual stability was found in Al cluster anions containing 13, 23, and 37 atoms by oxygen-etching experiments (6). Additionally, the Al_{13} cluster was evidenced to behave like a Cl atom (7–9). Subsequently, in the past decade, extensive investigations have been undertaken to explore and synthesize superatoms using various electron counting rules, and many superatoms have been found that can mimic the

chemical properties of halogens, alkaline earth metals, alkalis, and so on (3–5, 7, 10).

In the periodic table, REs are a series of chemical elements found in the Earth's crust that are vital to many modern technologies. One of the most valuable properties of the REs or rare earth-containing compounds is their optical characteristics, which have been widely applied in luminescent nanomaterials, generation and amplification of light in lasers, and optical amplifiers, etc. (11, 12). A popular example is the neodymium-doped yttrium aluminum garnet (Nd:YAG) laser (13), which is extensively used in many different fields. Equally important, because of the existence of localized unpaired f electrons, REs are very important components in magnetic materials (e.g., rare earth magnets $SmCo_5$ and NdFeB) and have attracted much attention recently (14–16). The mining process, however, is extremely damaging to the environment, resulting in the relatively small production, and the consequence is that REs are very expensive. Thus, our interest focuses on exploring novel superatomic clusters that can mimic the properties of the REs, which will be quite significant and valuable. Very recently, by using photoelectron imaging spectroscopy, we showed that the photoelectron spectra of diatomic clusters TiO^-, ZrO^-, and WC^- are very similar to those of their isovalent anions of group 10 elements, which are Ni^-, Pd^-, and Pt^-, respectively (1). Additionally, the similarity observed in these three isovalent counterparts indicates that, in a number of cases, various atom combinations can lead element mimics by using such a simple but effective isovalent counting rule. It was also found that the similar isovalent characterization and orbital occupation between superatomic clusters and the corresponding elements are two important factors in transition

Significance

Superatom concept has been found to be promising in designing atomic clusters to mimic the chemistry of scarce or expensive elements. Also, longstanding interest and challenge exist in searching for suitable candidates to mimic the valuable properties of rare earth elements owing to their highly important application in modern technologies and extremely low yield. Herein, by using photoelectron imaging spectroscopy, we provide direct experimental evidence that well-designed boron-doped clusters, namely LaB and NdB, could be promising candidates to mimic the magnetic properties of corresponding rare earth atoms Nd and Eu, respectively, because the same numbers of valence electrons, unpaired electrons, and magnetic moments are found in both of the counterparts. This finding opens up an exciting possibility for rare earth mimicry using the superatom concept.
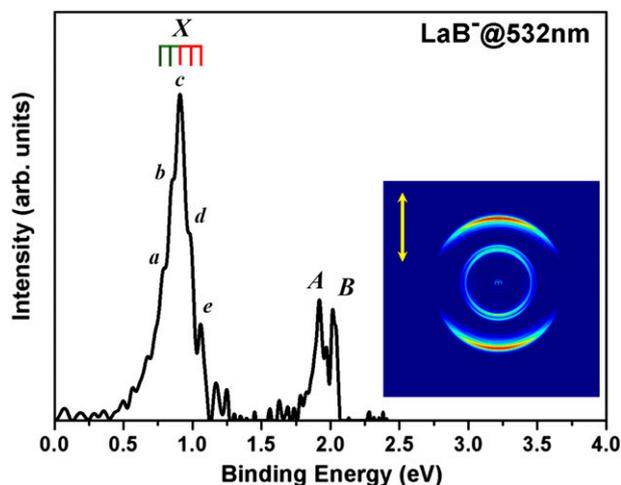
CHEMISTRY

Fig. 1. Photoelectron image and the corresponding photoelectron spectrum for the LaB⁻ cluster obtained at 532 nm.

metal mimicry (1, 17). These findings further motivate us to investigate the possibility of rare earth mimicry by using the superatom concept. Unlike the transition metals, as mentioned above, one of the most important properties of the REs is their magnetic characteristics owing to the abundant unpaired electrons. Therefore, finding a superatomic cluster with numbers of unpaired electrons and valence electrons that are similar to those of the corresponding RE is the most important step in mimicking the magnetic properties of REs, which is also the focus of this study. Spectroscopy combined with high-level theoretical calculations has been shown to be a powerful tool to directly examine the electronic structures of atoms and clusters (18–28). Herein, we used photoelectron imaging spectroscopy to explore the possibility of mimicking the magnetic properties of the REs.

Results and Discussion

In one of our recent studies about the electronic structures of the boron-doped lanthanum clusters (29), the number of unpaired electrons in neutral LaB was calculated to be four, which is identical to that of a rare earth atom Nd ([Xe] $4f^4$ $6s^2$). Additionally, the electron configurations of La and B are [Xe] $5d$ $6s^2$ and [He] $2s^2$ $2p$, respectively, and it was found that the B atom generally contributes its three valence electrons to the valence molecular orbitals of boron-doped rare earth clusters (29). Thus, the number of valence electrons of LaB is six, which is isovalent with Nd. These results imply that LaB may be a promising

Table 1. The calculated spin multiplicities, equilibrium bond lengths r_e (in angstroms), vibrational frequencies ω (in centimeters⁻¹), total energies (in hartree), and relative energies ΔE (in electronvolts) for the anionic and neutral LaB clusters

Species/spin multiplicity	r_e	ω	Total energy	ΔE
LaB⁻				
2	2.282	496.8	−460.328257	0.52
4	2.376	486.8	−460.347197	0.00
6	2.419	457.6	−460.319263	0.76
8	2.619	285.2	−460.144544	5.51
LaB				
1	2.088	634.8	−460.288064	0.57
3	2.202	470.5	−460.292743	0.45
5	2.325	524.5	−460.309126	0.00
7	2.435	386.1	−460.159995	4.06

Table 2. Experimental and theoretical ADEs and VDEs of the LaB⁻ and NdB⁻ diatomic clusters

Species	ADE		VDE	
	Experimental*	Theoretical	Experimental*	Theoretical
⁴LaB⁻	0.909 (25)	0.947	0.909 (25)	0.957
⁷NdB⁻	0.940 (22)	0.941	1.046 (16)	0.965

Energies are given in units of electronvolts.
*Numbers in parentheses represent experimental uncertainties in the last digits.

candidate to mimic the magnetic property of the rare earth Nd based on the discussion above. Therefore, photoelectron spectroscopy experiments are urgently required to verify this theoretical prediction. The photoelectron image and the corresponding photoelectron spectrum of LaB⁻ obtained at 532 nm are displayed in Fig. 1. The laser polarization is vertical in the image plane, which is indicated by a double yellow arrow in Fig. 1. The rings in the velocity map image correspond to different peaks in the photoelectron spectrum. As shown in Fig. 1, three prominent bands are observed below 2.33 eV (marked as X, A, and B) in the photoelectron spectrum of LaB⁻. Band X locates at the lower-binding energy region of the spectrum, featuring discernible vibrational structures. The most intense peak (c) in this band represents the transition from the ground state of LaB⁻ to the corresponding neutral electronic ground state, and the vertical detachment energy (VDE) of this band is measured to be 0.909 ± 0.025 eV. Other peaks in this band, which are a, b, d, and e, denote vibrationally resolved transitions. Peaks d and e stem from the transitions between the anion vibrational ground state and the υ = 1 and 2 vibrational energy levels of the ground state of LaB, respectively, yielding an experimental vibrational frequency of 532.3 cm⁻¹ for neutral LaB. Hot bands (peaks a and b) are also found in the lower-binding energy region with respect to the electron affinity (EA) -defined peak (c), which most likely comes from the transitions from the anion υ' = 2 and 1 vibrational levels of the LaB⁻ cluster to the ground vibrational state of LaB. A vibrational frequency of 467.8 cm⁻¹ of the LaB⁻ cluster is obtained from the peak spacing. Thus, based on the vibrationally resolved spectrum, the adiabatic detachment energy (ADE) of LaB⁻ is measured to be about 0.909 ± 0.025 eV, which is also the EA of neutral LaB. In addition, as shown in Fig. 1, another two strong transitions appear at the higher-binding energy region (labeled as A and B), which most probably come from the removal of deeper electrons producing the neutral cluster in vibrationally or electronically excited states.

To get more insights in the electronic structures of the neutral and anionic LaB clusters, high-level theoretical calculations have been performed to investigate the lowest-energy geometries of the clusters. Various spin states of the clusters were attempted, and the theoretical results are listed in Table 1. Based on these calculations, the ground state of LaB⁻ possesses a quartet state, whereas that of the LaB cluster features a quintet spin multiplicity, which is the same as that of the rare earth Nd. The theoretical bond lengths for the anionic and neutral LaB clusters are estimated to be about 2.376 and 2.325 Å, respectively. Moreover, to validate our calculated lowest-energy geometries of the anionic and neutral LaB clusters, the theoretical ADE and VDE of LaB⁻ were computed to compare with the experimentally measured values. It is worth noting that such a comparison is particularly helpful in diagnosing the accuracy of the theoretically proposed structures and bonding mechanisms (27, 30, 31). The theoretical ADE and VDE values of the LaB⁻ clusters are 0.947 and 0.957 eV, respectively, calculated at the CCSD(T) level of theory, and summarized in Table 2. As evidenced in Table 2, theoretical results are in good agreement with the experimental

Cheng et al.

Fig. 2. Photoelectron image and the corresponding photoelectron spectrum for the NdB$^-$ cluster obtained at 532 nm.

values. In addition, the theoretical vibrational frequencies of the neutral and anionic LaB clusters are calculated to be about 524.5 and 486.8 cm^{-1} (Table 1), respectively, which are very close to the experimental data (532.3 and 467.8 cm^{-1}) mentioned earlier. All of these findings give us confidence that the calculated ground-state structures of the clusters are correct, providing unambiguous experimental evidence that the spin multiplicity of the neutral LaB cluster is five. This result clearly verifies that four unpaired electrons exist in the diatomic LaB neutral cluster, which is same as that of Nd, implying that the magnetic moments for these two species are equal. Additionally, the numbers of the valence electrons in LaB and Nd are same (6 e$^-$) as discussed above. It is reasonable to suggest, therefore, that the isovalent LaB cluster could be a good candidate to mimic the magnetic property of the rare earth Nd, because both of them have the same numbers of valence electrons, unpaired electrons, and magnetic moments.

To verify it is not a mere coincidence in the LaB/Nd case, we also investigated whether such similarity is preserved between another boron-doped cluster NdB by simply doping a B atom into an Nd atom and its isovalent Eu ([Xe] $4f^7 6s^2$) atom. Fig. 2 shows the photoelectron image and the corresponding photoelectron spectrum of NdB$^-$ acquired at 532 nm. The ADE and VDE of the NdB$^-$ cluster are measured to be about 0.940 ± 0.022 and 1.046 ± 0.016 eV, respectively, from the EA defined peak (X) in Fig. 2, and they are also listed in Table 2. As shown in Fig. 2, other than peak X, a hot band, marked as X', locates at the lower-binding energy region. Additionally, several resolved peaks appear at the higher-binding energy region with respect to the peak X, which probably come from the detachment of deeper electrons forming the neutral cluster in electronically excited states. Accurate assignment of these peaks requires higher-level ab initio theoretical methods considering the excited states, which are beyond the scope and the focus of this study. Similarly, theoretical calculations have also been accomplished to examine the electronic structures of the anionic and neutral NdB clusters, and related results are listed in Table 3. Based on our theoretical calculations, the spin multiplicity for the lowest-energy geometry of NdB is eight, indicating that there are seven unpaired electrons involved in the cluster, which is the same as that of Eu. The accuracy of our calculated ground states of the clusters is validated from the good agreement between the experimental and theoretical ADE and VDE values of the NdB$^-$ cluster, which are displayed in Table 2. It is evident that the rare earth Eu and its isovalent NdB cluster have the same numbers of unpaired electrons

(7 e$^-$) as well as the same magnetic moments. Thus, the situation is surprisingly similar in the case of the Eu/NdB pair compared with the Nd/LaB pair, representing another example showing the possibility to mimic the magnetic properties of the REs using the superatom concept. The numbers of valence electrons, unpaired electrons, and magnetic moments for the diatomic clusters and corresponding REs studied here are summarized in Table 4. The similarity in both of the Nd/LaB and Eu/NdB cases is evidenced, enabling these diatomic clusters to be potential and valuable candidates to mimic the magnetic properties of the REs. Furthermore, it is worth mentioning that the abundance of the Eu element is considerably rarer than that of Nd. Therefore, we propose that the superatomic NdB cluster observed here could be an advantageous substitute for the rare Eu element regarding magnetic applications.

In addition, it is interesting to note that, according to the experimental findings observed here, it seems that the number of unpaired electrons in a diatomic boron-doped lanthanide cluster, namely LnB (Ln indicates a lanthanide atom), may be simply defined as $N_u(LnB) = N_u(Ln) + 3$, where $N_u(LnB)$ is the number of unpaired electrons of the diatomic cluster, $N_u(Ln)$ is the number of unpaired electrons of the Ln atom, and 3 equals the number of valence electrons of the B atom ([He] $2s^2 2p$). Taking the NdB cluster as an example, the $N_u(NdB)$ is seven (Table 4), which equals to the sum of $N_u(Nd)$ [$N_u(Nd)$ is four since Nd atom has four unpaired f electrons] and three. This counting rule is also valid in the case of LaB. Therefore, it seems that the three valence electrons of the boron atom just participate in the unpaired poll of the Ln atoms after doping the B atom into Ln forming the diatomic LnB cluster. Such a simple counting rule, which we name it as the "magic boron" counting rule here, may be used as a tool to estimate the spin characteristics of the diatomic LnB clusters, although the universality of this rule in the whole LnB group needs additional verification experimentally and theoretically. We wish this counting rule could be extended to other boron-containing clusters, and it will be useful in designing superatomic clusters to mimic the magnetic properties of elements in the periodic table.

Conclusion

In this study, by combining the velocity map imaging technique and high-level theoretical calculations, we have explored the possibility of using superatomic clusters to mimic the magnetic properties of the REs using the superatom concept. Considering the well-known magnetic characteristics of the REs, we suggest a strategy of designing clusters that have similar valence electrons and magnetic moments to the corresponding REs, which may

Table 3. The calculated spin multiplicities, equilibrium bond lengths r_e (in angstroms), vibrational frequencies ω (in centimeters^{-1}), total energies (in hartree), and relative energies ΔE (in electronvolts) for the anionic and neutral NdB clusters

Species/spin multiplicity	r_e	ω	Total energy	ΔE
NdB$^-$				
1	2.175	482.6	−585.987321	4.26
3	2.586	297.9	−586.141141	0.07
5	2.381	360.4	−586.092114	1.41
7	2.489	279.4	−586.143767	0.00
9	2.459	419.9	−586.133069	0.29
NdB				
2	2.722	300.0	−585.982479	3.57
4	2.643	249.1	−586.023199	2.47
6	2.378	393.8	−586.107600	0.17
8	2.371	408.2	−586.113775	0.00
10	2.472	353.2	−585.998251	3.14

Table 4. The numbers of valence electrons, unpaired electrons, and magnetic moments for two comparison pairs (namely ^{5}LaB/^{5}Nd and ^{8}NdB/^{8}Eu)

Species	Valence electron	Spin multiplicity	Unpaired electron	Magnetic moment
^{5}LaB	6	5	4	$4\mu_B$
^{5}Nd	6	5	4	$4\mu_B$
^{8}NdB	9	8	7	$7\mu_B$
^{8}Eu	9	8	7	$7\mu_B$

lead similar properties used as magnetic materials. Two diatomic boron-doped clusters, namely LaB and NdB, were observed to have the same numbers of valence electrons and unpaired electrons as those of the rare earth atoms Nd and Eu, respectively, enabling them to be promising candidates to achieve the objective in rare earth mimicry. The main goal of this study is to provide an original idea and direct experimental evidence to show the possibility in mimicking the rare earth group. Because mimics having similar spin characteristics have been found, another question regarding the preservation of their spin states or magnetic properties in cluster-assembled nanomaterials arises. To shed light on this point, more detailed study needs to be done by investigating the possibility of replacing the REs in larger rare-earth doped magnetic materials by these superatomic clusters. Additionally, because this study shows the possibility of mimicking the magnetic properties of REs, it will be even more interesting if one can design nonrare earth clusters to mimic the magnetic and other valuable properties (e.g., optical characteristics) of the REs, which are the future directions of our focus and also, exciting challenges in cluster science.

Materials and Methods

Experimental Details. In brief, the diatomic cluster anions LaB$^-$ and NdB$^-$ investigated here were produced in a laser vaporization source, where a 532-nm second harmonic Nd:YAG laser was used to ablate the 0.25-inch pure lanthanum and neodymium rods, respectively. A high-purity helium gas (typically 50 psi) seeded with 0.1% diborane gas was used as a carrier gas to produce boron-doped clusters, and the anionic species produced were mass analyzed using a time-of-flight mass spectrometer (32). The second harmonic of an Nd:YAG laser (532 nm) was used for photodetaching excess electrons from anions. Subsequently, photoelectrons were accelerated toward position-sensitive detectors, where the resulting 2D velocity distribution was recorded with a CCD camera. Finally, the 3D distribution was reconstructed from the photoelectron image using the BASEX and pBASEX programs (33, 34), which yielded similar results. The photoelectron spectrum was calibrated against the known spectrum of Bi$^-$ (35).

Computational Methods. All calculations presented here were accomplished using the Gaussian 09 program (36). To determine the ground-state structures and spin characteristics of the neutral and anionic clusters studied here, different spin multiplicity states were considered and fully optimized without symmetry constraints. The neutral and anionic LaB and NdB clusters were optimized using the density functional theory with hybrid functional B3LYP (37, 38). The augmented correlation consistent polarized triple-zeta valence (aug-cc-PVTZ) basis set was used to describe the atomic orbital of boron (39, 40), whereas the SDD (Stuttgart-Dresden effective core potential) with the Stuttgart-type small core (28 core electrons) and relativistic effective core potential was used for the Nd atom (41, 42). The method and basis sets used here have been proven to successfully predict the electronic structures of similar boron-doped lanthanide clusters (29). To reinforce the ground-state structures and take into account the zero-point energy correction, vibrational frequencies of different clusters were also calculated. The ADE was obtained by computing the energy difference between the anionic and neutral ground states, whereas the VDE was calculated as the energy difference between the neutral and anionic clusters (both at the ground-state geometry of the anion). Furthermore, the coupled cluster singles and doubles with perturbative contributions of connected triplets, CCSD(T) (43, 44) method with the same basis set was used to refine the ADE and VDE values of the ground-state structures.

1. Peppernick SJ, Gunaratne KDD, Castleman AW, Jr (2010) Superatom spectroscopy and the electronic state correlation between elements and isoelectronic molecular counterparts. *Proc Natl Acad Sci USA* 107(3):975–980.
2. Hunt ST, Nimmanwudipong T, Román-Leshkov Y (2014) Engineering non-sintered, metal-terminated tungsten carbide nanoparticles for catalysis. *Angew Chem Int Ed* 53(20):5131–5136.
3. Castleman AW, Jr (2011) From elements to clusters: The periodic table revisited. *J Phys Chem Lett* 2(9):1062–1069.
4. Luo Z, Castleman AW, Jr (2014) Special and general superatoms. *Acc Chem Res* 47(10):2931–2940.
5. Jena P (2013) Beyond the periodic table of elements: The role of superatoms. *J Phys Chem Lett* 4(9):1432–1442.
6. Leuchtner RE, Harms AC, Castleman AW, Jr (1989) Thermal metal cluster anion reactions: Behavior of aluminum clusters with oxygen. *J Chem Phys* 91(4):2753–2754.
7. Bergeron DE, Castleman AW, Jr, Morisato T, Khanna SN (2004) Formation of Al$_{13}$I$^-$: Evidence for the superhalogen character of Al$_{13}$. *Science* 304(5667):84–87.
8. Khanna SN, Jena P (1994) Designing ionic solids from metallic clusters. *Chem Phys Lett* 219(5–6):479–483.
9. Li X, Wu H, Wang XB, Wang LS (1998) *s-p* hybridization and electron shell structures in aluminum clusters: A photoelectron spectroscopy study. *Phys Rev Lett* 81(9):1909–1912.
10. Bergeron DE, Roach PJ, Castleman AW, Jr, Jones NO, Khanna SN (2005) Al cluster superatoms as halogens in polyhalides and as alkaline earths in iodide salts. *Science* 307(5707):231–235.
11. Carlos LD, Ferreira RAS, Bermudez VdeZ, Ribeiro SJL (2009) Lanthanide-containing light-emitting organic-inorganic hybrids: A bet on the future. *Adv Mater* 21(5):509–534.
12. Shen J, Sun LD, Yan CH (2008) Luminescent rare earth nanomaterials for bioprobe applications. *Dalton Trans* 42:5687–5697.
13. Geusic JE, Marcos HM, Van Uitert LG (1964) Laser oscillations in Nd-doped yttrium aluminum, yttrium gallium and gadolinium garnets. *Appl Phys Lett* 4(10):182–184.
14. Sessoli R, Powell AK (2009) Strategies towards single molecule magnets based on lanthanide ions. *Coord Chem Rev* 253(19–20):2328–2341.
15. Hughes ID, et al. (2007) Lanthanide contraction and magnetism in the heavy rare earth elements. *Nature* 446(7136):650–653.
16. Lips F, et al. (2012) Doped semimetal clusters: Ternary, intermetalloid anions [Ln@Sn$_7$Bi$_7$]$^{4-}$ and [Ln@Sn$_4$Bi$_9$]$^{4-}$ (Ln = La, Ce) with adjustable magnetic properties. *J Am Chem Soc* 134(2):1181–1191.
17. Tyo EC, Castleman AW, Jr, Reber AC, Khanna SN (2011) Analogous reactivity of Pd$^+$ and ZrO$^+$: Comparing the reactivity with small hydrocarbons. *J Phys Chem C* 115(34):16797–16802.
18. Bopp JC, et al. (2007) Spectroscopic characterization of the isolated SF$_6^-$ and C$_4$F$_8^-$ anions: Observation of very long harmonic progressions in symmetric deformation modes upon photodetachment. *J Phys Chem A* 111(7):1214–1221.
19. Bonačić-Koutecký V, Mitrić R, Werner U, Wöste L, Berry RS (2006) Ultrafast dynamics in atomic clusters: Analysis and control. *Proc Natl Acad Sci USA* 103(28):10594–10599.
20. Hansen JC, Duncanson JA, Jr, Chien RL, Berry RS (1980) Angular distributions of photoelectrons from resonant two-photon ionization of sodium through the 3p $^2P_{3/2}$ intermediate state. *Phys Rev A* 21(1):222–233.
21. Wang XB, et al. (2001) The electronic structure of CuCl$_2$ and CuBr$_2$ from anion photoelectron spectroscopy and ab initio calculations. *J Chem Phys* 114(17):7388–7395.
22. Schröder D, Schwarz H, Milko P, Roithová J (2006) Dissociation routes of protonated toluene probed by infrared spectroscopy in the gas phase. *J Phys Chem A* 110(27):8346–8353.
23. Yang X, Wang XB, Vorpagel ER, Wang LS (2004) Direct experimental observation of the low ionization potentials of guanine in free oligonucleotides by using photoelectron spectroscopy. *Proc Natl Acad Sci USA* 101(51):17588–17592.
24. Grubisic A, et al. (2011) Photoelectron spectroscopic and computational studies of the Pt@Pb$_{10}^{1-}$ and Pt@Pb$_{12}^{1-/2-}$ anions. *Proc Natl Acad Sci USA* 108(36):14757–14762.
25. Anderson SL, Rider DM, Zare RN (1982) Multiphoton ionization photoelectron spectroscopy: A new method for determining vibrational structure of molecular ions. *Chem Phys Lett* 93(1):11–15.
26. Cheng SB, Castleman AW, Jr (2014) Joint photoelectron imaging spectroscopic and theoretical characterization on the electronic structures of the anionic and neutral ZrC$_2$ clusters. *J Phys Chem A* 118(34):6935–6939.

27. Cheng SB, Berkdemir C, Melko JJ, Castleman AW, Jr (2014) S-P coupling induced unusual open-shell metal clusters. *J Am Chem Soc* 136(13):4821–4824.
28. Cheng S, Berkdemir C, Melko JJ, Castleman AW, Jr (2013) Probing the electronic structures and relative stabilities of monomagnesium oxide clusters MgO_x^- and MgO_x (x = 1-4): A combined photoelectron imaging and theoretical investigation. *J Phys Chem A* 117(46):11896–11905.
29. Cheng SB, Berkdemir C, Castleman AW, Jr (2014) Observation of d-p hybridized aromaticity in lanthanum-doped boron clusters. *Phys Chem Chem Phys* 16(2):533–539.
30. Melko JJ, et al. (2010) Anion photoelectron spectroscopy and first-principles study of Pb_xIn_y clusters. *J Phys Chem C* 114(48):20907–20916.
31. Gupta U, Reveles JU, Melko JJ, Khanna SN, Castleman AW, Jr (2010) Origins of stability in mixed bismuth-indium clusters. *J Phys Chem C* 114(38):15963–15972.
32. Wiley WC, McLaren IH (1955) Time-of-flight mass spectrometer with improved resolution. *Rev Sci Instrum* 26(12):1150–1157.
33. Dribinski V, Ossadtchi A, Mandelshtam VA, Reisler H (2002) Reconstruction of abel-transformable images: The Gaussian basis-set expansion abel transform method. *Rev Sci Instrum* 73(7):2634–2642.
34. Garcia GA, Nahon L, Powis I (2004) Two-dimensional charged particle image inversion using a polar basis function expansion. *Rev Sci Instrum* 75(11):4989–4996.
35. Andersen T, Haugen HK, Hotop H (1999) Binding energies in atomic negative ions: III. *J Phys Chem Ref Data* 28(6):1511–1533.
36. Frisch MJ, et al. (2009) *Gaussian 09* (Gaussian Inc., Wallingford, CT), Rev A.01.
37. Lee C, Yang W, Parr RG (1988) Development of the Colle-Salvetti correlation-energy formula into a functional of the electron density. *Phys Rev B Condens Matter* 37(2):785–789.
38. Becke AD (1993) Density-functional thermochemistry. III. The role of exact exchange. *J Chem Phys* 98(7):5648–5652.
39. Kendall RA, Dunning TH, Jr, Harrison RJ (1992) Electron-affinities of the first-row atoms revisited. Systematic basis sets and wave functions. *J Chem Phys* 96(9):6796–6806.
40. Dunning TH, Jr (1989) Gaussian basis sets for use in correlated molecular calculations. I. The atoms boron through neon and hydrogen. *J Chem Phys* 90(2):1007–1023.
41. Cao X, Dolg M (2001) Valence basis sets for relativistic energy-consistent small-core lanthanide pseudopotentials. *J Chem Phys* 115(16):7348–7355.
42. Dolg M, Stoll H, Preuss H (1989) Energy-adjusted *ab initio* pseudopotentials for the rare earth elements. *J Chem Phys* 90(3):1730–1734.
43. Purvis GD III, Bartlett RJ (1982) A full coupled-cluster singles and doubles model: The inclusion of disconnected triples. *J Chem Phys* 76(4):1910–1918.
44. Raghavachari K, Trucks GW, Pople JA, Head-Gordon M (1989) A fifth-order perturbation comparison of electron correlation theories. *Chem Phys Lett* 157(6):479–483.

CHEMISTRY